Submersion of sodium impurities in finite cryogenic droplets: A path-integral molecular dynamics study for ^{4}He and para-H_2

F. Calvo*
Université Grenoble Alpes, LIPHY, F-38000 Grenoble, France
and CNRS, LIPHy, F-38000 Grenoble, France
(Received 6 September 2016; published 30 January 2017)

The size-dependent submersion of sodium clusters into helium and para-hydrogen droplets has been computationally investigated using continuum models and path-integral molecular dynamics (PIMD) simulations. All-atom explicit potential energy surfaces combining a semiempirical many-body model for the alkali-metal subpart and a pairwise additive repulsion-dispersion contribution for the solvent-alkali-metal interactions parametrized on quantum chemical calculations were employed for the simulations. Direct evidence for the submersion process was found by placing a sufficiently large sodium cluster, Na_{55}, initially at the surface of a $^4He_{300}$ droplet, whereas Na_{13} spontaneously migrates to the surface when initially placed at the center of this droplet. Under the normal fluid conditions probed by our approach, submersion in larger helium droplets appears thermally activated but the potential of mean force harvested from out-of-equilibrium PIMD trajectories confirms that the submersion transition occurs near the size of 20 atoms, in agreement with earlier investigations. In the case of para-hydrogen media, temperature and the crystalline nature of the cryogenic host were both found to play significant roles: while a single sodium atom migrates to the surface of liquid p-H_2 clusters, it remains stuck inside at 2 K. Similarly, a Na_{13} cluster remains at the surface in a cold p-H_2 cluster but becomes readily submerged at 16 K. Our results also indicate that submersion is disfavored in smaller droplets of the cryogenic medium.

DOI: 10.1103/PhysRevB.95.035429

I. INTRODUCTION

Cryogenic media such as helium droplets or hydrogen matrices are convenient to achieve high-resolution spectroscopy of complex molecular dopants. The very weak interactions with the media, the sharp spectral features provided by the low temperature, and, in the case of crystalline hosts, the suppression of rotational motion all combine to enable exceptional laboratory conditions that are similar to those found in astrophysical environments as diverse as interstellar clouds, icy grains, or cometary tails [1]. In addition, the properties and superfluidity of the solvent can be revealed by probing the impurity [2].

In general the dopant of interest binds to the solute more strongly than the solute itself, especially since intrasolute interactions in helium or para-hydrogen are further damped by zero-point motion. This occurs naturally for ions, which are strongly bound by polarization forces, but also for instance organic molecules or neutral molecular complexes. Nonwetting with helium droplets is known to notably occur for alkali-metal atoms, owing to the strong Pauli repulsion between their active s electron and the closed valence clouds of the rare gas atoms [3]. Several experimental and theoretical studies have highlighted the importance of the interactions between the impurity and the solvent in this case, revealing that the equilibrium shape on the ground electronic state is that of an exterior alkali-metal atom forming a dimple on the droplet [4–6], Pauli repulsion also acts for alkali-metal clusters; however, when such clusters are formed from individual atoms on the droplet the energy released upon metallic bond formation depends on the spins involved in this bond. This phenomenon leads to the preferential formation of high-spin clusters on the droplet, low spin systems being ejected as their greater formation energy is dissipated into solvent evaporation.

Larger alkali-metal clusters are most likely to reside in their ground electronic state [7,8] but interact more strongly with the cryogenic host as the dispersion attraction and the polarizability increase with the number of metal atoms. Hence above some size the cluster is expected to become submerged into the droplet and reside in a bubble caused by Pauli repulsion. Following earlier efforts by Ancilotto and co-workers [9], the energetic balance between (advantageous) submersion and (penalizing) creation of the bubble was analyzed theoretically by Stark and Kresin [10], who reported critical sizes for submersion in the range of 8–131 depending on the alkali metal and the isotopic nature of helium. These theoretical predictions were confirmed by electron spectroscopy measurements by An der Lan and co-workers, who concluded that the transition between surface and submerged locations occurs above 20 atoms for sodium [11], and above 80 atoms for potassium [12]. Additional measurements carried out by the same group [13] have also found that the submersion transition is strongly affected by the presence of a polarizable dopant molecule in the droplet such as C_{60}.

The theoretical analyses by Stark and Kresin [10] emphasize the various physical phenomena responsible for the submersion process. In order to yield tractable equations especially in the many-body treament of van der Waals interactions, this work employed continuous models, assumed the clusters to be spherical and fully metallic, and the helium droplet to be infinite, some approximations that may not hold for very small systems at low temperature. Sodium clusters are indeed spherical but usually when they are liquid, low-energy

*florent.calvo@univ-grenoble-alpes.fr

structures turning out to be quite deformed [14,15], sometimes due to Jahn-Teller distortion [14]. In addition, characteristic electron delocalization expected for a metal may not be fully achieved in such "molecules" in which the electronic structure is highly discrete [16]. In the case of sodium, clusters containing fewer than 170 atoms were estimated to become metallic only above room temperature [17]. Finally, although helium droplets contain a large number of atoms (millions or more), they do not strictly represent a bulk medium and finite size effects may not be negligible owing to the long range of the dispersion interaction.

The question of submersion also arises for the hydrogen solvent. Sodium in contact with H_2 reacts only at high temperatures to form hydrides [18], and under cryogenic conditions the sodium atom was predicted by Ancilotto and co-workers [9] to submerge readily into liquid hydrogen. In this case, the interaction potential employed to determine the equilibrium location of the alkali-metal impurity was partly phenomenological. Obviously, larger sodium clusters are then also expected to be submerged. However, in contrast with helium droplets, clusters of para-hydrogen crystallize at sufficiently low temperature [19] and this could kinetically hinder submersion.

The purpose of the present paper is to offer a complementary theoretical perspective on the problem of size-induced submersion of sodium clusters into helium droplets and para-hydrogen clusters, operating at the atomistic level through path-integral molecular dynamics (PIMD) simulations employing realistic potential energy surfaces, and accounting for different temperatures under possibly different states of the cryogenic host. Using an additive model for the sodium cluster-solvent interactions, we find indeed that while Na_{13} spontaneously migrates to the exterior of a small ^{4}He droplet, the Na_{55} cluster is readily submerged. Extending the analysis by Stark and Kresin [10], the results are also found to depend on the size of the helium droplet, and such size effects are also noted upon adapting the additive continuum model to finite cryogenic media. Free-energy calculations carried out in a larger droplet confirm that 20 sodium atoms are close to the critical size of the submersion transition, in accordance with earlier predictions [10] and experimental measurements [11]. We have also revisited the Na-H_2 interaction by performing quantum chemistry calculations and found it to be substantially weaker than in the early work by Ancilotto *et al.* [9], making submersion of the single sodium atom much less likely than anticipated earlier. Submersion of Na clusters appears in this case as a size-dependent process as well, but our simulations also confirm the intuitive finding that if the para-hydrogen cluster is solidlike it can trap the sodium cluster at metastable locations, the crossover for the submersion transition being shifted to larger effective sizes.

The article is organized as follows. In the next section we describe the general computational methodology employed to simulate sodium clusters interacting with helium or para-H_2 clusters, and give details about the interaction potentials. While the basic PIMD approach is already well documented [20,21], additional techniques were employed to speed up these expensive simulations and are also briefly reviewed. Continuous models along the lines of those developed by Stark and Kresin [10], here treated in the same additive approximation of sodium-solvent interactions as used in the atomistic simulations but extended to treat finite solvent droplets, are also made more explicit in Sec. II. The results for the ^{4}He and para-H_2 media assuming normal (nonsuperfluid) conditions are given in Secs. III and IV, respectively. A general discussion and some concluding remarks close the article in Sec. V.

II. COMPUTATIONAL METHODS

The approach followed in this work relies on the atomistic modeling of both sodium and cryogenic clusters in contact with each other, and their simulation at finite temperature in which nuclear quantum effects are accounted for through the PIMD method. Performing these simulations requires accurate potential energy surfaces for the various interactions, primarily for the Na-He and Na-H_2 partners.

A. Path-integral molecular dynamics

Aiming to simulate realistic helium or hydrogen clusters containing at least hundreds of particles, only few methods are available to treat such large systems by taking into account their quantum mechanical nature, including the efficient but approximate approaches based on quantum-corrected potentials [22], the Feynman-Hibbs expansion [23], or quantum thermal baths [24,25]. The PIMD method used here is rigorous and includes vibrational delocalization and tunneling, although lacking bosonic exchange effects in its standard version. It is not our purpose to review here the PIMD approach beyond the basic ingredients given below, further details being available in recent papers [20,21].

The system of interest is denoted as Na_nX_p, with X = ^{4}He or H_2 assimilated as a point particle, and the total number of particles is referred to as $N = n + p$ for simplicity. This structureless approximation for para-H_2 molecules is justified by the free rotations they experience in their $J = 0$ state at the low pressures of finite clusters in vacuum, giving rise to isotropic rotational wave functions [26]. In the PIMD approach the classical particles are replaced by a number P of monomers forming a polymer necklace, each monomer acting as an imaginary time slice along the thermal path in the path integral theory [23]. The position of monomer α ($1 \leqslant \alpha \leqslant P$) of particle i ($1 \leqslant i \leqslant N$) is denoted as $\mathbf{r}_{\alpha,i}$ together with the cyclic condition $\mathbf{r}_{P+1,i} = \mathbf{r}_{1,i}$. The monomers interact successively through harmonic bonds, in such a way that the equilibrium quantum mechanical state is approximated by that of the classical but higher-dimensional system of $N \times P$ particles driven by the effective potential

$$V_{\rm eff}(\mathbf{R}) = \frac{1}{P}\sum_{\alpha=1}^{P} V(\mathbf{R}_\alpha) + \sum_{\alpha=1}^{P}\sum_{i\in\text{particles}} \frac{m_i P}{2\beta^2\hbar^2}\|\mathbf{r}_{\alpha,i} - \mathbf{r}_{\alpha+1,i}\|^2, \quad (1)$$

where we have also denoted $\mathbf{R}_\alpha$ the collective set of coordinates for monomer α, and simply $\mathbf{R}$ the entire set of $N \times P$ coordinates. In this equation $\beta = 1/k_{\rm B}T$ with T the temperature and $k_{\rm B}$ the Boltzmann constant, $\hbar$ is the reduced Planck constant and m_i the mass of particle i.

In the PIMD method the thermally equilibrated configurations at temperature T are obtained by coupling the system to massive Nosé-Hoover thermostats [27], and the variables are transformed into normal modes in order to decouple the harmonic part of the Hamiltonian [20,21]. PIMD trajectories were propagated using the velocity Verlet integrator [28] with a time step of 1 fs and over a total simulated time ranging between 100 and 1000 ps.

Traditional PIMD trajectories were conducted with initial conditions chosen specifically with the sodium dopant at various locations within or outside the cryogenic host, the spontaneous motion of the cluster within the simulated time straightforwardly giving insight into its relative stability. Note that the PIMD method we are using is a pure equilibrium method not designed for addressing the true kinetics of the submersion or ejection processes. In larger helium clusters, and as discussed in more details below, no significant motion could be detected under the simulated time, the submerged and exterior configurations appearing both locally stable. While the relative quantum energies could still be evaluated using the standard virial estimator [29] or higher-order schemes [30], we also attempted to determine the potential of mean force of the cluster as a function of its distance from the center of the helium droplet. We use here the same method based on out-of-equilibrium driven trajectories, as pioneered by Hummer and Szabo [31] in the classical case and extended to the path-integral framework by Hernández de la Peña and co-workers [32,33]. The method consists of adding a time-dependent umbrella potential $\delta V(\mathbf{R}_\alpha)$ centered at a position that varies linearly with time, progressing from the center to the exterior of the droplet or reversely as

$$\delta V(\mathbf{R}) = \tfrac{1}{2}k[r_{ab} - d(t)]^2, \tag{2}$$

in which r_{ab} is the distance between the centers of mass of the two clusters, $d(t) = d_0 + \lambda t$ is a linearly varying function of time t, and k a fixed spring constant. The potential of mean force $\mathcal{F}(r_{ab})$ at temperature T is obtained from the work $W(t)$ accumulated at time t as [31,32]

$$\mathcal{F}(r_{ab}) = \mathcal{F}_0 - k_\mathrm{B}T\ \ln\langle\delta(r'_{ab} - r_{ab}) \times \exp(-\beta[W(t) - \delta V(r'_{ab})])\rangle \tag{3}$$

and

$$W(t) = \int_0^t \frac{\partial \delta V}{\partial d}\frac{\partial d}{\partial t'}dt' = k\lambda\int_0^t [d(t') - r_{ab}]dt'. \tag{4}$$

In Eq. (3), $\mathcal{F}_0$ is an unimportant additive constant and the angular brackets denote a canonical average over different initial conditions. In the context of PIMD simulations, and as in a previous study [34], the biasing potential δV was added only to the centroid normal mode variables. It could also have applied to each ring-polymer bead but for a higher and unnecessary computational cost. 100 independent driven trajectories were carried out by pulling the sodium cluster away from the center, initial conditions being sampled with a strong harmonic potential keeping $d(t) = 0$.

Each out-of-equilibrium PIMD trajectory was propagated for 10^5 time steps of 1 fs, with a spring constant k taken as 10^{-4} atomic units.

B. Potential energy surfaces

The systems under scrutiny are highly heterogeneous with the two clusters possibly moving relative to each other. The total interaction potential V is partitioned into the following components:

$$V = V_\mathrm{Na} + V_\mathrm{X} + V_\mathrm{Na-X}, \tag{5}$$

where V_Na is the potential energy of the pure sodium cluster, V_X the interaction of the helium or hydrogen cryogenic host, and $V_\mathrm{Na-X}$ the interaction between the two clusters.

At the very low temperatures considered here, approaching 10 K or below, the alkali-metal cluster is expected to lie in its electronic and vibrational ground state, and could thus probably even be described as a harmonic system. Instead we have chosen a simple analytical but reasonable many-body potential of the Gupta form [35] to model the interactions in these clusters. The parameters presently used for sodium were adjusted on solid state properties, and are thus especially valid at low temperature [36]. The interaction between helium atoms was taken as the Janzen-Aziz pair potential [37]. For para-H_2, the Silvera-Goldman potential [38] in its "isolated form" was used to model the interaction between a pair of structureless H_2 molecules. This potential was shown to reproduce quantitatively the equilibrium solid phase of para-hydrogen [39].

As correctly pointed out by Stark and Kresin [10], the true interaction between extended systems having delocalized electrons entails complex many-body effects involving the dielectric function of each component and their respective boundaries. At present such an approach appears untractable for molecular simulation, although recent progress for related problems should be noted [40]. In addition, the extent of electron delocalization in a very small finite system with only few valence electrons responsible for the metallic character at cryogenic temperatures is probably more limited; hence we assume an additive pairwise form for the interaction between the two clusters, the interactions among sodium atoms remaining as a many-body contribution.

To calibrate the potentials, we have performed electronic structure calculations at the level of coupled cluster theory with single, double, and perturbative triple excitations and the aug-cc-pv5z basis set. For Na-H_2, several calculations were performed for different orientations of the H_2 molecule relative to the axis joining its center mass to the Na atom, and subsequently averaged. Quantum chemical calculations were carried out using the GAUSSIAN09 software package [41].

The Na-He and Na-H_2 interactions in their corresponding ground electronic states are depicted in Fig. 1 as a function of the interparticle distance. For both systems, the interaction is about half as strong as the interaction between two solute particles. The Na-He potential is extremely weak, and can be satisfactorily represented by a simple Lennard-Jones potential with well depth $\varepsilon = 1.58$ K and distance parameter $\sigma = 5.99$ Å. Our calculations agree with the recent quantum chemical study of Dell'Angelo and co-workers at the CASSCF level [42]. We also notice a reasonable agreement (within 10%) with the earlier LJ parameters reported by Ancilotto *et al.* [9] also used by Stark and Kresin [10]. However, it is interesting to evaluate how the conclusions reached by these authors are affected

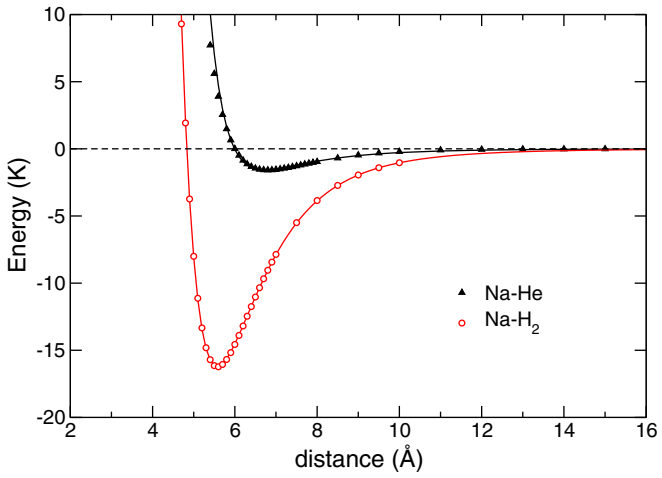

FIG. 1. Ground state potential energy versus interparticle separation for a sodium atom interacting with a helium atom (black triangles) or a hydrogen molecule (red circles), after averaging over orientations. The symbols are the results of quantum chemistry calculations at the CCSD(T) level; the continuous lines depict the analytical potentials used to represent these interactions.

by employing such expectedly more accurate values of the interaction parameters.

Turning now to the Na-H_2 interaction, the equivalent LJ parameters are found to be $\varepsilon = 16.29$ K and $\sigma = 4.83$ Å, at more severe variance with the data used by Ancilotto and co-workers [9] who reported a well depth of 30 K. The weaker binding predicted by our calculations is likely to influence the conclusions reached by these authors who predicted that a single sodium atom would readily submerge into liquid H_2, further motivating our own investigation. A similar form as the Silvera-Goldman potential used to model H_2-H_2 interactions was employed to model the interaction between Na and H_2 molecules. Using the same variable names as in the original paper [38], parameters that accurately represent the CCSD(T) data are (all in atomic units) $\alpha = 1.3577251$, $\beta = 1.0428$ bohr^{-1}, $\gamma = 0$, $C_6 = 146.3412$, $C_8 = 1538.3406$, and $C_{10} = 0$.

The additive nature of the interaction between the two clusters further allows us to use a ring contraction technique [43] to alleviate a significant part of the computational burden by reducing the number of beads needed to describe subparts of the system. With this rigorous trick only a set of $P' < P$ lower frequency normal modes are considered when describing the heavier and more tightly bound sodium cluster, hence the $V_{\rm Na}$ and $V_{\rm Na-X}$ interactions, whereas the helium or para-H_2 cluster itself, the $V_{\rm X}$ term as well as all dynamical variables are described using P monomers [43]. In this work P' was always chosen to be equal to 8, whereas P was taken as 128 for ^{4}He at $T = 1$ K (normal fluid state), $P = 256$ for H_2 at $T = 2$ K, and $P = 32$ at $T = 16$ K. To ensure that these values are appropriate, we present in Appendix B the evolution of the quantum energies of selected systems with increasing P or P'.

C. Additive continuum models

It is instructive to compare the simulation results to the predictions of continuum models, as developed and used by Ancilotto *et al.* [9] and, more recently, in a more sophisticated version that includes many-body screening effects in the van der Waals energy, by Stark and Kresin [10]. In the present work we assume additive interactions between Na and cryogenic particles and the LJ potential to represent these interactions for both systems. The more accurate Silvera-Goldman potential for Na-H_2, although relevant in the simulations, is not prone to analytical integration in the continuum models.

Following Stark and Kresin [10], we start by considering the two situations of a *spherical* sodium cluster (density $\rho_{\rm Na}$) either in contact with a flat semi-infinite solvent surface (density $\rho_{\rm X}$) or submerged into a bulk solvent with the same density. The values for the densities are taken as in Refs. [9,10]. For a given number n of sodium atoms, the cluster radius is simply obtained from $R(n) = r_{\rm S} n^{1/3}$ with the Wigner-Seitz radius of sodium $r_{\rm S} = 3.93$ Å [10,44].

Assuming pairwise additive LJ interactions of the form $V(r) = C_{12}/r^{12} - C_6/r^6$ between the continuous media, the total energy for a spherical cluster with radius R and whose center is distant from the flat surface by the distance d reads [10]

$$\begin{aligned} V_{\rm exterior}(R;d) &= C_{12} W_{12}(R;d) - C_6 W_6(R;d), \\ W_{12}(R;d) &= \frac{5R-d}{(d-R)^7} + \frac{7R+d}{(d+R)^7}, \\ W_6(R;d) &= \frac{R}{d-R} + \frac{R}{d+R} - \ln\frac{d+R}{d-R}, \end{aligned} \tag{6}$$

which must be minimized to get the optimal distance d and the corresponding equilibrium energy $V_{\rm exterior}^{\rm (min)}$.

In the submerged case, the cluster with radius R creates a cavity with radius $d > R$, the formation of the cavity entailing a penalty in the total energy equal to

$$V_{\rm cavity}(d) = 4\pi\sigma(d) d^2, \tag{7}$$

and where we have denoted $\sigma(d)$ the surface tension which additionally depends on the radius through the traditional expression [9]

$$\sigma(d) = \sigma_{\rm X}\left(1 - \frac{\Delta_{\rm X}}{d}\right). \tag{8}$$

The bulk surface tension $\sigma_{\rm He}$ and the Tolman length $\Delta_{\rm He}$ for ^{4}He were taken as in Ref. [10]. For H_2, and as Ancilotto and co-workers [9] we borrow the surface tension value from the known properties at the triple point, $\sigma_{H_2} = 2.06$ K Å^{-2}. However, in the absence of known reliable data for the Tolman length, we have performed two sets of calculations with $\Delta_{H_2} = 0.1$ bohr and $\Delta_{H_2} = 1$ bohr.

The integrated LJ energy of the spherical cluster with radius R in the cavity with radius d reads

$$\begin{aligned} V_{\rm submerged}(R;d) &= 4\pi^2 \rho_{\rm X}\rho_{\rm Na}[C_{12} W_{12}(R;d) - C_6 W_6(R;d)], \\ W_{12}(R;d) &= \frac{1}{45}\left[\frac{R^2}{8(d-R)^8} - \frac{R^2}{8(R+d)^8}\right. \\ &\quad + \frac{R}{28(d-R)^7} - \frac{R}{28(R+d)^7} \\ &\quad \left. + \frac{1}{168(d-R)^6} - \frac{1}{168(R+d)^6}\right] \end{aligned}$$

$$+\frac{1}{40}\left[\frac{R}{7(d-R)^7}+\frac{R}{7(R+d)^7}\right.$$
$$\left.-\frac{1}{42(d-R)^6}+\frac{1}{42(R+d)^6}\right],$$
$$W_6(R;d)=\frac{1}{6}\left[\frac{R^2}{2(d-R)^2}-\frac{R^2}{2(R+d)^2}\right.$$
$$\left.-\frac{R}{R+d}-\frac{R}{d-R}-\ln\frac{d-R}{R+d}\right]$$
$$+\frac{1}{4}\left[\frac{R}{d-R}+\frac{R}{R+d}\ln\frac{R+d}{d-R}\right]. \quad (9)$$

Similar to the exterior case, for a given cluster radius R the total energy $V_{\text{submerged}}+V_{\text{cavity}}$ must be minimized as a function of d. The critical submersion size n^* is obtained from comparing this energy to V_{exterior}, the radius R being related to the size n through $n=4\pi\rho_{\text{Na}}R^3/3$.

The dependence of solute properties on the amount of solvent has been recognized in biomolecular chemistry [45], and here we have examined this issue as well, by extending the additive continuum models so they can describe *finite* solvent droplets having n_X particles. By assuming spherically symmetric shapes, the integrations can still be carried out exactly and the details are provided in Appendix A.

III. SODIUM DOPANTS IN HELIUM DROPLETS

The predictions of the additive continuum model for the interaction energy of a sodium cluster Na_n submerged inside or lying at the surface of a helium droplet having $n_{\text{He}}=10^3$, 10^4 atoms and in the infinite size limit are shown in Fig. 2. The variations of both $V_{\text{submerged}}+V_{\text{cavity}}$ and V_{exterior} obtained by minimizing Eq. (6) or Eqs. (7) and (9) together, respectively, as well as their equivalent formulas for finite helium droplets, are shown as a function of n. As already discussed by Stark and Kresin [10], such a simple additive continuum model already captures the size-induced submersion transition by predicting that sufficiently large clusters are better accommodated in a fully solvated state. With the presently made approximations, especially the additive nature of the cluster-solvent interactions, the critical size for the transition in the bulk helium limit is evaluated to take place as low as $n^*=5$ atom, clearly at variance with the previous conclusions reached in Refs. [10,11]. Repeating the calculations with the exact LJ parameters employed by Stark and Kresin [10] does not solve this discrepancy, which thus results from the more sophisticated treatment devoted by these authors to the dispersion energy. However, if we now include the finite extension of the helium droplet, then the continuum models appear to predict quantitatively different sizes with the submerged configuration being slightly disfavored and n^* taking the values of 7 and 6 for 10^3 and 10^4 He atoms, respectively. Yet, convergence to the bulk limit is reached relatively fast, approximately for 10^6 atoms which is close to the actual size of experimentally produced helium droplets.

We can now discuss the atomistic results of the path-integral MD trajectories, first considering the basic situation of two clusters Na_n and He_p initially placed in contact either on the side or as a submerged alkali-metal cluster. For these preliminary simulations we set n to 13 or 55 and take the clusters in their Mackay icosahedral global minima for the present potential [15], and $p=300$ or 500 corresponding to medium size helium clusters. The pure He_p cluster is sampled at thermal equilibrium for 10 ps, and the sodium impurity is placed next to it in such a way that the minimum Na-He distance exceeds 3 Å, or in the submerged case by creating a large enough cavity at the center, also imposing a minimum distance of 3 Å between Na and He atoms, helium atoms being moved from the center to the surface of the droplet accordingly.

The distances between the centers of mass of the two clusters have been monitored as a function of time. Fig. 3(a)

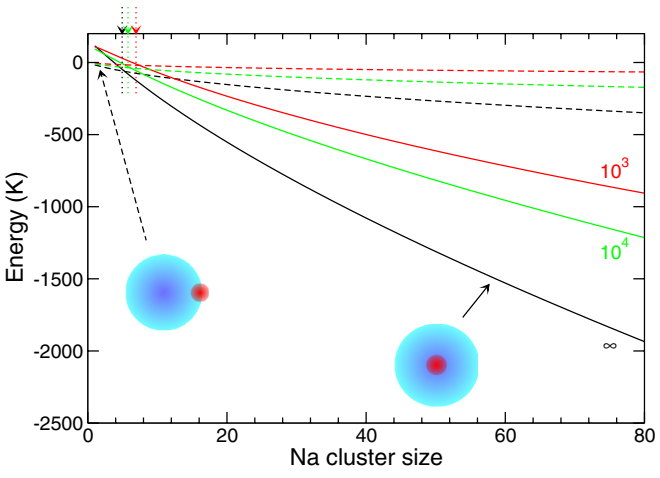

FIG. 2. Energy of a sodium cluster Na_n adsorbed next to (black dashed line) or inside (red solid line) a helium droplet as a function of n and for two finite helium droplets having 10^3 and 10^4 atoms and in the infinite size limit, as predicted by the corresponding additive continuum models (see text for details). The vertical arrows point at the different crossover sizes obtained for the different helium droplet sizes.

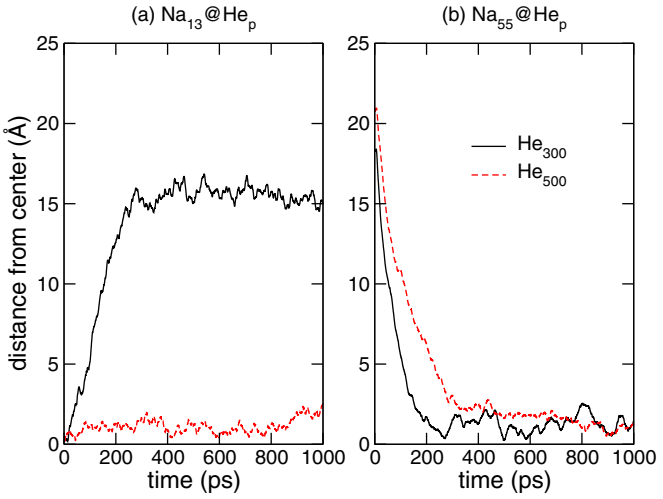

FIG. 3. Distance between the centers of mass of a Na_n cluster in contact with a ^4He_p droplet obtained in PIMD trajectories, for $p=300$ (solid black lines) or 500 (dashed red lines). (a) Na_{13} initially at the center of the droplet; (b) Na_{55} initially at the edge of the droplet.

shows their variations in the case of Na_{13} initially submerged in the helium droplets while Fig. 3(b) shows the corresponding data for Na_{55} initially at the surface of the two droplets, as obtained from typical PIMD trajectories. In the case of the smaller cluster He_{300}, the two sodium clusters clearly exhibit contrasted behaviors with Na_{13} spontaneously migrating to the exterior and Na_{55} being readily submerged, in both cases under typical times of 200 ps. Again, the presently employed computational methodology does not strictly give insight into the true dynamics of the submersion or ejection processes; hence these numbers should be taken only as indicative. However, in the case of the larger helium cluster He_{500}, and while Na_{55} still drowns inside, the 13-atom sodium cluster now remains submerged. Repeating these trajectories three times does not alter these results qualitatively and confirms that the spontaneous submersion or ejection of the alkali-metal cluster depend on the size of the helium droplet. Shorter simulations performed for the Na_{13} cluster but employing the much less spherical minimum reported by Poteau and Spiegelman [14] using a quantum tight-binding model predict the very same behavior, with the cluster being ejected in the smaller helium droplet. These results indicate a limited effect of the sodium cluster shape on the submersion process. The numerical observations of a preferential submersion in larger droplets are also consistent with the results from the extended continuum model.

These preliminary results provide a direct illustration of the size-dependent submersion transition of Na clusters in helium droplet, and confirm that the critical size lies between 13 and 55 sodium atoms. They also already point out at several issues overlooked so far. First, despite a strictly identical interaction potential considered in the PIMD simulations and in the additive continuum model, there is a significant discrepancy in the transition size which appears underestimated in the continuum approach. Secondly, these results neglect the role of the solvent size, which according to our continuum calculations could become important below a few thousand particles.

PIMD simulations of the Na_{13} cluster at the surface of the He_{500} cluster indicate, unsurprisingly, that the alkali-metal impurity stays comfortably outside and has a lower quantum energy by about 150 K relative to the submerged situation shown in Fig. 3(a). Therefore, a barrier must exist to prevent spontaneous dissociation of the cluster under the nanosecond time scale. In a true superfluid helium environment the dynamics would probably be strongly affected and the sodium clusters able to travel across the helium host much easier. However this remains somewhat speculative since there is presently no efficient method to address the quantum dynamics of such many-body systems that fully include exchange statistics and properly treat the bosonic character of ^{4}He. Moreover, we note that the superfluid nature of helium would not alter the predictions of continuous models [9,10].

Under the normal fluid conditions, the barrier preventing spontaneous submersion or ejection can be evaluated using driven PIMD trajectories, and reconstructing the potential of mean force from the work exerted by the biasing force [31]. Using this methodology we have collected the results of 100 independent trajectories of selected Na_n clusters initially submerged at the center of the He_{1000} cluster and ejected away

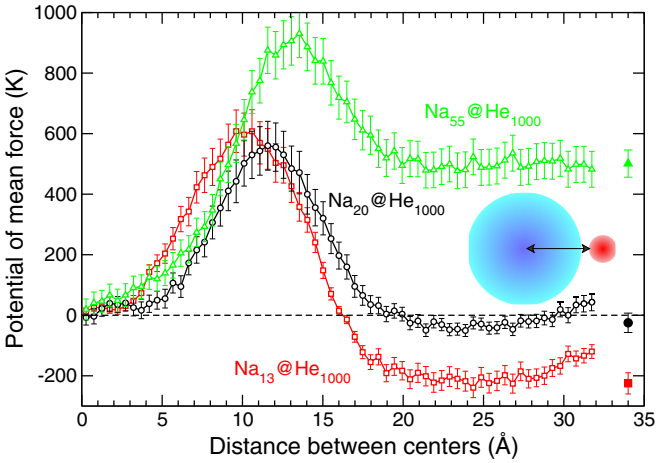

FIG. 4. Potential of mean force of $Na_n@He_{1000}$ as a function of intercluster separation, as obtained from out-of-equilibrium PIMD trajectories for $n = 13$ (red empty squares), $n = 20$ (black empty circles), and $n = 55$ (blue empty triangles). The full symbols indicate the quantum energy of the surface configuration relative to the submerged configuration obtained from unbiased PIMD trajectories, for the same corresponding clusters.

from it. The resulting data obtained for Na_{13}, Na_{55} but also Na_{20} are shown in Fig. 4. The potentials of mean force show a common generic trend, with a broad barrier extending over about 6–7 Å and reaching 600–1000 K depending on the specific alkali-metal cluster. The exterior configurations are respectively more, nearly equally as, and less stable than the submerged configuration as the size increase from 13 to 20 and finally 55. In Fig. 4 we have also reported the relative quantum energies of the exterior configuration with respect to the submerged configuration, as obtained from unbiased PIMD simulations for the same three clusters. The differences in equilibrium energies satisfactorily match the potential of mean force differences between the corresponding states, which validates our computational protocol for calculating the PMF.

The results of Fig. 4 can be discussed in the light of the normal PIMD trajectories in which the small Na_{13} cluster was found to be stuck inside He_{500} despite being more stable outside. The barrier to be crossed for Na_{13} from the submerged configuration is significantly higher than the one for Na_{55} coming from the exterior, which is consistent with the asymmetry in the spontaneous migration noted for the latter system in Fig. 3(b). Besides these two border sizes, the case of Na_{20} appears as intermediate, with very similar energies in the exterior and submerged configurations, slightly in favor of the former. Although we have not considered cluster sizes other than 20, this result confirms the predictions of Stark and Kresin [10] supported by the experimental measurements of An der Lan *et al.* [11] that the critical size for submersion in ^{4}He is indeed close to 20 sodium atoms and possibly slightly larger.

The overall agreement between the three studies may partly be fortuitous on our side, because despite having clearly shown that Na_{13} and Na_{55} behave in opposite ways our investigation has also highlighted some role in the size of the helium droplet. Repeating the PMF calculations for He_{500} instead of

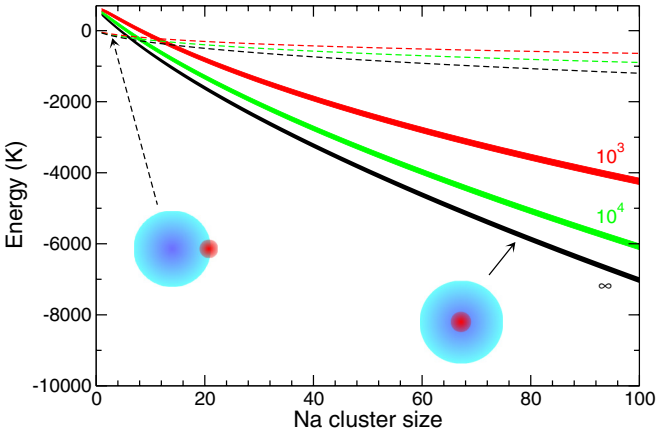

FIG. 5. Energy of a sodium cluster Na_n adsorbed next (black dashed line) or inside (red solid line) a para-H_2 droplet as a function of n and for two finite hydrogen droplets having 10^3 and 10^4 molecules and in the infinite size limit, as predicted by the corresponding additive continuum models (see text for details). The thick lines drawn for the submerged case correspond to the uncertainty on the Tolman length of para-hydrogen.

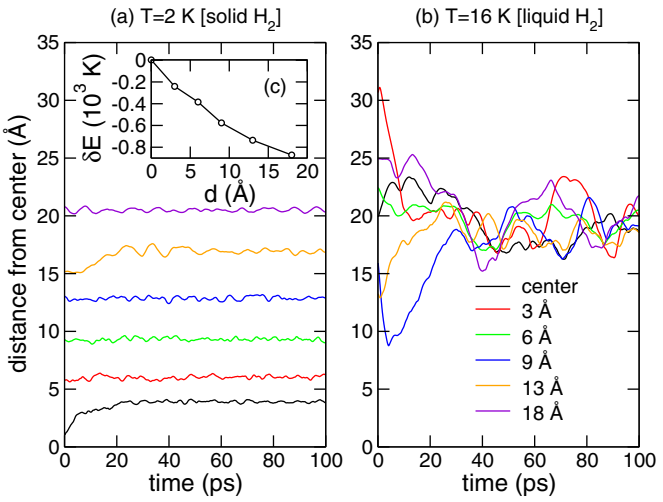

FIG. 6. Time variations of the distance between a single Na impurity and the center of the $(p\text{-}H_2)_{560}$ cluster, assuming different initial locations of this impurity, as obtained from PIMD trajectories at different temperatures. (a) $T = 2$ K; (b) $T = 16$ K. The inset (c) shows the relative quantum energies of the configurations at 2 K as a function of the initial distance to the center.

He_{1000} shows very similar trends but barriers that are reduced by 100–200 K (results not shown). More significantly, the relative energy differences between submerged and exterior configurations remain in the same range and do not vary by more than 20% than the values reported in Fig. 4. That the droplet size influences more the barrier and the kinetics than the relative configurational stability suggests that our computational results should remain relatively robust and apply also to more realistic droplets containing several thousands of atoms.

IV. SODIUM DOPANTS IN PARA-HYDROGEN CLUSTERS

Sodium atoms were predicted by Ancilotto and co-workers to submerge into liquid hydrogen under cryogenic conditions [9]; however, the interaction parameters used by these authors differ significantly from those obtained in the present work based on quantum chemical calculations. The key role of this interaction appears clearly on the variations of the cluster energies in the submerged and exterior cases with cluster size, as predicted by the additive continuum model in Fig. 5, again for the two finite sizes of 10^3 and 10^4 para-H_2 molecules and in the bulk limit. As expected, the general behavior found for the para-H_2 solvent is similar to the one for ^{4}He. In the bulk droplet limit and with the present interaction parameters, sodium clusters having six atoms or less are predicted to remain at the surface of the droplet. As the cryogenic droplet shrinks, this critical size increases up to about 12 molecules for $n_{H_2} = 1000$. In all cases the sodium monomer is thus found to be preferentially at the surface, but clusters of 13 atoms or more should be submerged.

Obviously the continuum approximation is not expected to be very realistic at such extremely small sizes, whereas the atomistic PIMD approach is naturally sound. We have first considered the case of a single Na impurity inside or outside a medium size para-H_2 cluster at the two temperatures of $T = 2$ and 16 K, below and above the melting temperature of molecular hydrogen. In the solidlike state, the hydrogen cluster host can be expected to adopt icosahedral shapes at least up to several thousands of molecules [46]. We have chosen here the convenient size of 561 molecules forming six Mackay icosahedral shells, and substituted one of them with the sodium atom at different distances from the center, before locally relaxing the configurations and running the PIMD trajectories. The time variations of the distance between the sodium atom and the center of the hydrogen cluster at the two temperatures are represented in Figs. 6(a) and 6(b). Here the effects of the temperature and the thermodynamical state of the host cluster are found to be quite drastic. In contact with a liquid H_2 droplet, the atomic impurity spontaneously migrates to the border, at variance with the analysis of Ancilotto and co-workers based on a stronger interaction potential but also assuming a liquid host [9].

In contrast, the impurity remains near its starting position if the hydrogen cluster is solidlike, diffusion at such a low temperature of 2 K being essentially suppressed under the time scale of the simulation. The relative energies obtained from the virial expression, also reported in Fig. 6(c), vary steadily with the distance from the center and show that the nonwetted configuration is significantly more stable than the submerged monomer.

According to the continuum model and conversely to the monomer, the Na_{13} cluster should spontaneously submerge into molecular hydrogen. We have thus performed additional PIMD simulations for the $Na_{13}(p\text{-}H_2)_{1000}$ system under the two thermodynamical conditions, placing the sodium cluster either outside the hydrogen cluster or making room for it in a central cavity. At this size, the starting configuration of the H_2 cluster was taken again as multilayer icosahedral, and the simulations were performed at 2 or 16 K. These simulations were also longer, covering 1 ns after the initial 10 ps equilibration period.

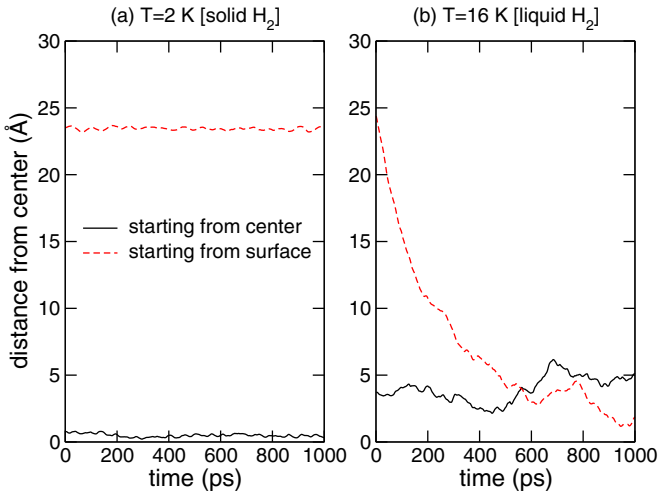

FIG. 7. Time variations of the distance between the Na_{13} cluster and the center of the $(p\text{-}H_2)_{560}$ cluster, for submerged or exterior initial conditions and as obtained from PIMD trajectories at different temperatures. (a) $T = 2$ K; (b) $T = 16$ K.

The time variations of the distance between the two clusters centers of mass after this equilibration period are represented in Fig. 7. Similar to the single atom impurity, solid para-hydrogen clusters are able to trap the larger sodium cluster in its initial position quite efficiently. However, the submerged configuration is now more stable than the exterior configuration by about 670 K, which indicates that submersion should take place but over time scales that far exceed the nanosecond. Diffusion in the liquid hydrogen droplet is of course much faster and can be directly seen on the spontaneous immersion of the cluster now occurring on hundreds of picoseconds only.

Our modeling thus indicates that the size-dependent submersion transition also occurs for the hydrogen host, the critical size for submersion being lower than 13 atoms. We have not tried to locate this value more precisely, which for this system could be close to the predictions of the simple continuum model and lie near seven sodium atoms. However, in view of the more significant kinetic effects obtained for the crystalline systems, we can also anticipate the transition not to be sharp as in a fluidlike host, but to occur through a broader range of sizes which are likely to be trapped owing to the slow diffusion.

V. DISCUSSION AND CONCLUSIONS

The nonwetting of sodium atoms or small clusters on ^{4}He or para-H_2 droplets results from their extremely weak mutual interaction, which grows as either of the two clusters enlarges. The dependence on alkali-metal cluster size is of primary interest, because it describes its preferential submersion occurring above some critical size. However, the present results have also highlighted some possible dependence on the host droplet size, already at the level of only a few hundreds of particles which are far below the experimental size of actual helium nanodroplets that is closer to millions of atoms [1].

The continuum model previously employed by Ancilotto *et al.* [9] and Stark and Kresin [10], used here in its additive version but adapted to the slightly different interaction parameters of the atomistic simulations, still underestimates the critical transition size for ^{4}He. However, its extension to finite solvent droplets has revealed significant size effects for small droplets containing fewer than about 10^5 particles that tend to disfavor submersion. Although not straightforward, it would be interesting to refine the approach of Stark and Kresin to determine the extent of droplet size effects on the critical size in a nonadditive description of van der Waals interactions.

The droplets investigated in our numerical experiments contain only hundreds of atoms, at which the extended continuum model yields a submersion transition near seven sodium atoms. Our path-integral simulation results directly confirm the size-dependent submersion process, but estimate the transition to occur near 20 atoms, precisely close to the predictions of Stark and Kresin [10] and to the recent experimental measurements by the Scheier group [11]. The agreement could thus partly originate from the possible overestimation of van der Waals energies due to the neglect of screening effects compensating the finite size effects involving the droplet size. As suggested above, one related issue is that the importance of these screening effects is likely dependent on the droplet size, which precisely is not (semi-)infinite in practice.

The superfluid nature of the helium droplet, neither accounted for in earlier or the present continuum modelings [9,10] nor in the PIMD simulations, should not drastically affect the general conclusions regarding relative energetic stability, although it is likely to alter the barrier for submersion found in the present calculations for large enough helium droplets in the normal fluid state. Unfortunately, it currently appears rather difficult to incorporate these effects in the atomistic approach due to the large size of the systems under scrutiny and the added complexity of sampling the exchange paths among the ring polymers [47,48]. Additional path-integral Monte Carlo simulations [47] could help assessing the importance of the bosonic nature of the helium solvent on the relative energetic stability of submerged and exterior configurations, especially near the transition size. For droplets in the normal fluid state, our calculations suggest that a barrier exist for submersion; hence the well-defined critical size should be replaced by a critical *range* of a few atoms over which it would be possible to observe both exterior and submerged metastable configurations.

In the case of hydrogen hosts, our predictions are at variance with those from Ancilotto and co-workers [9] for the single sodium atom, and also provide evidence for a size-dependent submersion transition taking place below 13 sodium atoms. However, at very low temperatures the hydrogen cluster is nearly crystalline and hampers the submersion process dramatically, whereas spontaneous migration of single atoms to the liquid surface is anticipated. We also expect these results to convey to sodium clusters at the surface of bulk para-H_2, clusters even larger than the critical submersion size becoming likely trapped outside a crystalline parahydrogen matrix over a reasonably large range. Noteworthily, the continuum and atomistic approaches seem to better agree with each other for this cryogenic host than for helium. This is partly expected owing to the smaller size of the sodium cluster and its even less metallic character, but also to the much more heterogeneous

nature of molecular hydrogen compared to superfluid helium. If would of course be useful to verify the predictions of a size-dependent submersion process on molecular hydrogen experimentally, but also to extend this work to other alkali metals studied in Ref. [9].

This investigation also emphasized the possibly important kinetic aspects that could explain the metastability of submerged or exterior configurations, the PIMD trajectories being too short to allow for the spontaneous migration of the alkali-metal impurity away or inside through the cryogenic medium. Kinetics should naturally play a role in the case of metastable trapping of sodium aggregates outside crystalline para-hydrogen matrices or clusters. The migration kinetics in nonsuperfluid droplets could be addressed using specific path-integral approaches tailored for the approximate calculation of quantum time correlation functions such as centroid [49] or ring-polymer [50] molecular dynamics, combined with ideas from transition path sampling [51] designed for circumventing the rare event issue.

APPENDIX A: INTERACTION ENERGIES BETWEEN FINITE LENNARD-JONES SPHERES

In this Appendix we give the explicit formulas for the interactions between a sodium cluster and a cryogenic but *finite* droplet of helium or para-hydrogen, both assumed to be spherically symmetric and homogeneous with respective densities $\rho_{\rm Na}$ and $\rho_{\rm X}$, in the case where the interaction between sodium and the solvent particles are additive and of the Lennard-Jones form. The numbers of sodium and solvent particles are fixed as $N_{\rm Na}$ and $N_{\rm X}$, respectively.

We first consider the situation in which the sodium cluster is submerged at the center of a shell of solvent atoms, as depicted in Fig. 8(a). $N_{\rm Na}$ fixes $R_{\rm A}$, the radius of the sodium cluster, and the solvent is located in a shell between radii d and $R_{\rm B}$.

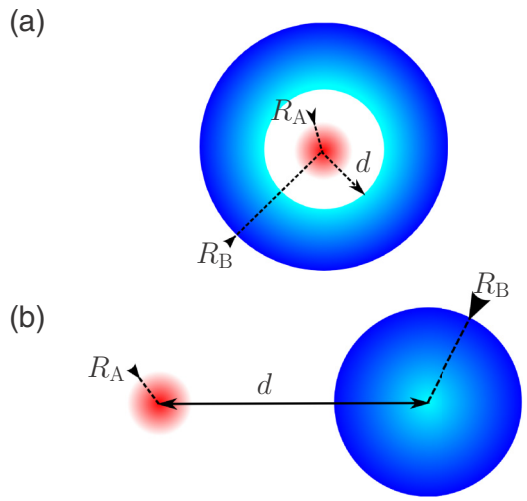

FIG. 8. Geometric definitions in the calculation of the integrated Lennard-Jones interaction between (a) a central sphere and an outer shell; (b) two spheres, all objects being homogeneous.

The solvent being incompressible, $N_{\rm X}$ fixes $R_{\rm B}$ as

$$R_{\rm B} = \left(\frac{3N_{\rm X}}{4\pi\rho_{\rm X}} + d^3\right)^{1/3}. \tag{A1}$$

For an elementary C_n/r^n potential between particles of the sodium cluster and of the solvent, the integration over the two volumes yields the total potential

$$\begin{aligned}
V_n(R_{\rm A},R_{\rm B},d) &= \frac{8\pi^2\rho_{\rm Na}\rho_{\rm X}C_n}{(n-2)(n-3)(n-4)}\Phi_n(R_{\rm A},R_{\rm B},d),\\
\Phi_n(R_{\rm A},R_{\rm B},d) &= R_{\rm A}[g_{n-5}(d,R_{\rm A}) + g_{n-5}(R_{\rm B},R_{\rm A})]\\
&\quad - \frac{1}{n-6}[f_{n-6}(d,R_{\rm A}) - f_{n-6}(R_{\rm B},R_{\rm A})]\\
&\quad + R_{\rm A}^2[f_{n-4}(d,R_{\rm A}) - f_{n-4}(R_{\rm B},R_{\rm A})],\\
f_p(d,R) &= \frac{1}{(d-R)^p} - \frac{1}{(d+R)^p},\\
g_p(d,R) &= \frac{1}{(d-R)^p} + \frac{1}{(d+R)^p},
\end{aligned}$$

and, for $n = 6$,

$$\begin{aligned}
\Phi_6(R_{\rm A},R_{\rm B},d) &= R_{\rm A}[g_1(d,R_{\rm A}) + g_1(R_{\rm B},R_{\rm A})]\\
&\quad - \frac{1}{6}[f_0(d,R_{\rm A}) - f_0(R_{\rm B},R_{\rm A})]\\
&\quad + R_{\rm A}^2[f_2(d,R_{\rm A}) - f_2(R_{\rm B},R_{\rm A})],\\
f_0(d,R) &= \ln\frac{d-R}{d+R}.
\end{aligned}$$

Although we have not tried to simplify these expressions further, they have the advantage of being easily verified numerically against the initial integrals.

In addition to the LJ interaction, the surface energies exerted on the inner (cavity) and outer surfaces of the solvent shell are expressed as

$$\begin{aligned}
V_{\rm cavity}(d) &= 4\pi d^2\sigma_{\rm X}\left(1 - \frac{\Delta_{\rm X}}{d}\right),\\
V_{\rm outer}(R_{\rm B}) &= 4\pi R_{\rm B}^2\sigma_{\rm X}\left(1 - \frac{\Delta_{\rm X}}{R_{\rm B}}\right),
\end{aligned}$$

respectively. For given sizes of the two clusters, $R_{\rm A}$ is fixed, and for a given d then $R_{\rm B}$ is fixed as well, the total energy of the system being finally written as a function of d as

$$\begin{aligned}
V_{\rm submerged}(d) &= 8\pi^2\rho_{\rm Na}\rho_{\rm X}\left[\frac{C_{12}}{720}\Phi_{12}(d) - \frac{C_6}{24}\Phi_6(d)\right]\\
&\quad + V_{\rm cavity}(d) + V_{\rm outer}(d).
\end{aligned} \tag{A2}$$

This expression generalizes Eqs. (9) and (7) to the case where the surrounding solvent has a finite width. It must be numerically minimized to obtain the optimal distance d and energy separating the two clusters in the submerged configuration.

Likewise, a similar procedure can be applied to the case depicted in Fig. 8(b) where the two clusters are in external contact with each other. This problem was previously also considered by Wu [52], and amounts to calculating the LJ potential between two spheres with radii $R_{\rm A}$ and $R_{\rm B}$ and

separated by the distance d between the centers of mass. The result for a C_n/r^n potential is now

$$V_n(R_A,R_B,d) = \frac{4\pi^2\rho_{Na}\rho_X C_n}{(n-2)(n-3)(n-4)(n-5)}\Psi_n(R_A,R_B,d),$$

$$\Psi_n(R_A,R_B,d) = \frac{1}{(n-7)d}[f_{n-7}(d-R_B,R_A) - f_{n-7}(d+R_B,R_A)] - \frac{R_A}{d}[g_{n-6}(d-R_B,R_A) - g_{n-6}(d+R_B,R_A)]$$
$$- \frac{1}{n-6}[f_{n-6}(d-R_B,R_A) - f_{n-6}(d+R_B,R_A)] - \frac{R_A^2}{d}[f_{n-5}(d-R_B,R_A) - f_{n-5}(d+R_B,R_A)]$$
$$+ R_A[g_{n-5}(d-R_B,R_A) - g_{n-5}(d+R_B,R_A)],$$

and, for the special case $n = 6$,

$$\Psi_6(R_A,R_B,d) = f_0(d-R_B,R_A) - f_0(d+R_B,R_A) - \frac{R_A^2}{d}[f_1(d-R_B,R_A) - f_1(d+R_B,R_A)]$$
$$+ R_A[g_1(d-R_B,R_A) - g_1(d+R_B,R_A)],$$

which for $R_A = R_B$ readily yields the expression first obtained by Hamaker [53,54]. In the general case $R_A \neq R_B$, we could not find compact expressions for the integrated LJ potential above, but we checked it is invariant upon the inversion $R_A \rightleftharpoons R_B$.

The finite radius of the solvent droplet also contributes to a surface energy equal to $V_{ref}(N_X)$ given by

$$V_{ref}(N_X) = 4\pi R_B^2\sigma_X\left(1 - \frac{\Delta_X}{R_B}\right),$$

and which does not depend on d. The expression for the total energy of the two spheres in exterior contact with each other that generalizes Eq. (6) is

$$V_{exterior}(d) = 4\pi^2\rho_{Na}\rho_X\left[\frac{C_{12}}{5040}\Psi_{12}(d) - \frac{C_6}{24}\Psi_6(d)\right] + V_{ref}, \tag{A3}$$

which again must be minimized against d to yield the minimum energy in the exterior configuration, to be compared to the optimal energy in the submerged case. In Figs. 2 and 5 the two energies are shown after removing the common contribution $V_{ref}(N_X)$ from the outer surface energy, as they would otherwise diverge with increasing size of the solvent droplet.

APPENDIX B: TROTTER CONVERGENCE

In the ring contraction approach, the Trotter numbers P and P' can be seen as associated with the solvent and sodium particles, respectively, even though P' is really an intermediate quantity that does not bear the same importance as P. To ensure that the PIMD trajectories correctly sample the nuclear wave function at the requested temperature, we present here the evolution of the quantum energies with increasing values of P at fixed P', and ensure that P' is appropriately chosen as well.

The quantum energies were evaluated using the standard virial estimator [29],

$$E_{virial} = \frac{3N}{2\beta} - \frac{1}{2P}\sum_{i=1}^{N}\sum_{\alpha=1}^{P}(\mathbf{r}_{\alpha,i} - \bar{\mathbf{r}}_i)\cdot\frac{\partial V}{\partial \mathbf{r}_{\alpha,i}} + \frac{1}{P}\sum_{\alpha=1}^{P}V(\mathbf{R}_\alpha), \tag{B1}$$

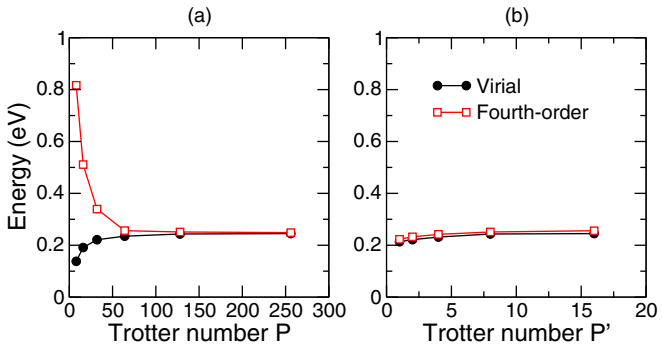

FIG. 9. Convergence of the total quantum energy of $Na_{13}He_{100}$ at $T = 1$ K with increasing Trotter numbers P and P' in the ring-contraction scheme. (a) Main number P at fixed $P' = 8$; (b) number P' at fixed $P = 128$. The full black circles and the empty red squares refer to energies obtained from the virial and the fourth-order corrected second-order energies, respectively. All energies are given relative to the classical equilibrium value obtained for $P = P' = 1$.

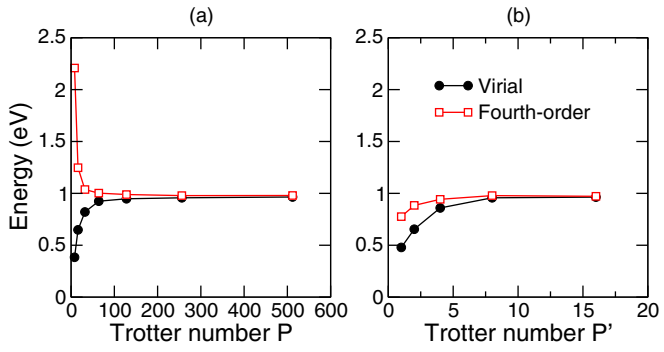

FIG. 10. Convergence of the total quantum energy of $Na_{13}(p\text{-}H_2)_{100}$ at $T = 2$ K with increasing Trotter numbers P and P' in the ring-contraction scheme. (a) Main number P associated at fixed $P' = 8$; (b) number P' at fixed $P = 256$. The full black circles and the empty red squares refer to energies obtained from the virial and the fourth-order corrected second-order energies, respectively. All energies are given relative to the classical equilibrium value obtained for $P = P' = 1$.

where $\bar{\mathbf{r}}_i$ is the centroid position for particle i, or using the fourth-order corrected primitive estimator [30],

$$\langle E_4 \rangle = \frac{\langle (E_2 + 3V_{\rm TI}) \exp(-\beta V_{\rm TI}) \rangle}{\langle \exp(-\beta V_{\rm TI}) \rangle}, \tag{B2}$$

where $V_{\rm TI}$ is the Takahashi-Imada [55] correction to the second-order expression of the effective potential of Eq. (1):

$$V_{\rm TI} = \frac{(\beta\hbar)^2}{24P^3} \sum_{i=1}^{N} \sum_{\alpha=1}^{P} \left(\frac{\partial V}{\partial \mathbf{r}_{\alpha,i}} \right)^2, \tag{B3}$$

and E_2 the traditional primitive or second-order estimator

$$E_2 = \frac{3NP}{2\beta} + \frac{1}{P} \sum_{\alpha=1}^{P} V(\mathbf{R}_\alpha) - \sum_{\alpha=1}^{P} \sum_{i=1}^{N} \frac{m_i P}{2\beta^2\hbar^2} \|\mathbf{r}_{\alpha,i} - \mathbf{r}_{\alpha+1,i}\|^2. \tag{B4}$$

In Fig. 9 we show how the quantum energy of $Na_{13}\,He_{100}$ at $T = 1$ K varies either with increasing P and fixed $P' = 8$, or with increasing P' and fixed $P = 128$. The energy is represented relative to the classically obtained result for $P = P' = 1$; hence it can be considered as the anharmonic zero-point energy contribution to the total quantum energy. Figure 10 shows the corresponding data for $Na_{13}(p\text{-}H_2)_{100}$ at $T = 2$ K.

For both systems, the convergence of the quantum energies with the main Trotter number P is smooth and occurs from below using the virial estimator, or from above with the (fourth-order corrected) primitive estimator. This bracketing behavior indicates anharmonic zero-point energies close to 0.245 eV and 0.965 eV for the helium and para-H_2 hosts, respectively. We find a very satisfactory convergence (within 2%) for $P = 128$ and 256 for the two systems.

[1] F. Stienkemeier and K. K. Lehman, J. Phys. B **39**, R127 (2006).
[2] M. Hartmann, R. E. Miller, J. P. Toennies, and A. Vilesov, Phys. Rev. Lett. **75**, 1566 (1995).
[3] F. Dalfovo, Z. Phys. D **29**, 61 (1994).
[4] F. Ancilotto and F. Toigo, Phys. Rev. B **50**, 12820 (1994).
[5] J. Reho, C. Callegari, J. Higgins, W. E. Ernst, K. K. Lehmann, and G. Scoles, Faraday Discuss. **108**, 161 (1997).
[6] F. Stienkemeier, O. Bünermann, R. Mayol, F. Ancilotto, M. Barranco, and M. Pi, Phys. Rev. B **70**, 214509 (2004).
[7] S. Vongehr and V. V. Kresin, J. Chem. Phys. **119**, 11124 (2003).
[8] O. Bünermann and F. Stienkemeier, Eur. Phys. J. D **61**, 645 (2011).
[9] F. Ancilotto, E. Cheng, M. W. Cole, and F. Toigo, Z. Phys. B **98**, 323 (1995).
[10] C. Stark and V. V. Kresin, Phys. Rev. B **81**, 085401 (2010).
[11] L. An der Lan, P. Bartl, C. Leidlmair, H. Schöbel, R. Jochum, S. Denifl, T. D. Märk, A. M. Ellis, and P. Scheier, J. Chem. Phys. **135**, 044309 (2011).
[12] L. An der Lan, P. Bartl, C. Leidlmair, H. Schöbel, S. Denifl, T. D. Märk, A. M. Ellis, and P. Scheier, Phys. Rev. B **85**, 115414 (2012).
[13] M. Renzler, M. Daxner, L. Kranabetter, A. Kaiser, A. W. Hauser, W. E. Ernst, A. Lindinger, R. Zillich, P. Scheier, and A. M. Ellis, J. Chem. Phys. **145**, 181101 (2016).
[14] R. Poteau and F. Spiegelmann, J. Chem. Phys. **98**, 6540 (1993).
[15] F. Calvo, S. Tran, S. A. Blundell, C. Guet, and F. Spiegelmann, Phys. Rev. B **62**, 10394 (2000), and references therein.
[16] W. A. de Heer, Rev. Mod. Phys. **65**, 611 (1993).
[17] B. von Issendorff and O. Cheshnovsky, Annu. Rev. Phys. Chem. **56**, 549 (2005).
[18] M. D. Banus and A. A. Hinckley, in *Handling and Uses of the Alkali Metals* (Adv. in Chemistry, American Chemical Society, Washington, DC, 1957), p. 106.
[19] G. Tejeda, J. M. Fernández, S. Montero, D. Blume, and J. P. Toennies, Phys. Rev. Lett. **92**, 223401 (2004).
[20] A. Pérez, M. E. Tuckerman, and M. H. Müser, J. Chem. Phys. **130**, 184105 (2009).
[21] S. Habershon, D. E. Manolopoulos, T. E. Markland, and T. F. Miller III, Annu. Rev. Phys. Chem. **64**, 387 (2013).
[22] D. Bonhommeau, P. T. Lake, C. Le Quiniou, M. Lewerenz, and N. Halberstadt, J. Chem. Phys. **126**, 051104 (2007).
[23] R. P. Feynman and A. Hibbs, *Quantum Mechanics and Path Integrals* (MacGraw-Hill, New York, 1965).
[24] M. Ceriotti, G. Bussi, and M. Parrinello, Phys. Rev. Lett. **103**, 030603 (2009).
[25] H. Dammak, Y. Chalopin, M. Laroche, M. Hayoun, and J.-J. Greffet, Phys. Rev. Lett. **103**, 190601 (2009).
[26] P. Sindzingre, D. M. Ceperley, and M. L. Klein, Phys. Rev. Lett. **67**, 1871 (1991).
[27] G. J. Martyna, M. L. Klein, and M. A. Tuckerman, J. Chem. Phys. **99**, 2796 (1993).
[28] G. J. Martyna, D. J. Tobias, and M. L. Klein, J. Chem. Phys. **101**, 4177 (1994).
[29] M. F. Herman, E. J. Bruskin, and B. J. Berne, J. Chem. Phys. **76**, 5150 (1982).
[30] A. Pérez and M. E. Tuckerman, J. Chem. Phys. **135**, 064104 (2011).
[31] G. Hummer and A. Szabo, Proc. Natl. Acad. Sci. USA **98**, 3658 (2001).
[32] R. van Zon, L. Hernández de la Peña, G. H. Peslherbe and J. Schofield, Phys. Rev. E **78**, 041103 (2008).
[33] L. Hernández de la Peña and G. H. Peslherbe, J. Phys. Chem. B **114**, 5404 (2010).
[34] F. Calvo, Phys. Rev. E **82**, 046703 (2010).
[35] R. P. Gupta, Phys. Rev. B **23**, 6265 (1981).
[36] Y. Li, E. Blaisten-Barojas, and D. A. Papaconstantopoulos, Phys. Rev. B **57**, 15519 (1998).
[37] A. R. Janzen and R. A. Aziz, J. Chem. Phys. **107**, 914 (1997).
[38] I. F. Silvera and V. V. Goldman, J. Chem. Phys. **69**, 4209 (1978).
[39] F. Operetto and F. Pederiva, Phys. Rev. B **73**, 184124 (2006).
[40] G. D. Förster, F. Rabilloud, and F. Calvo, Phys. Rev. B **91**, 245433 (2015); **92**, 165425 (2015).
[41] M. J. Frisch, G. W. Trucks, H. B. Schlegel, G. E. Scuseria, M. A. Robb, J. R. Cheeseman, G. Scalmani, V. Barone, B. Mennucci, G. A. Petersson *et al.*, Gaussian 09, Revision D.01, Gaussian, Inc., Wallingford, CT, 2009.

[42] D. Dell'Angelo, G. Guillon, and A. Viel, J. Chem. Phys. **136**, 114308 (2012).
[43] T. E. Markland and D. E. Manolopoulos, J. Chem. Phys. **129**, 024105 (2008).
[44] J. P. Toennies and A. F. Vilesov, Angew. Chem., Int. Ed. **43**, 2622 (2004).
[45] M. T. Sykes and M. Levitt, Proc. Natl. Acad. Sci. USA **104**, 12336 (2007).
[46] B. W. dan de Waal, J. Chem. Phys. **90**, 3407 (1989).
[47] D. M. Ceperley, Rev. Mod. Phys. **67**, 279 (1995).
[48] Ł. Walewski, H. Forbert, and D. Marx, Comput. Phys. Commun. **185**, 884 (2014).
[49] J. Cao and G. A. Voth, J. Chem. Phys. **99**, 10070 (1993).
[50] I. R. Craig and D. E. Manolopoulos, J. Chem. Phys. **121**, 3368 (2004).
[51] P. G. Bolhuis, D. Chandler, C. Dellago, and P. L. Geissler, Annu. Rev. Phys. Chem. **53**, 291 (2002).
[52] J.-J. Wu, J. Adhes. Sci. Technol. **26**, 251 (2012).
[53] H. C. Hamaker, Physica **4**, 1058 (1937).
[54] F. Calvo, M. Benali, V. Gerbaud, and M. Hemati, Computing Lett. **1**, 183 (2005).
[55] M. Takahashi and M. Imada, J. Phys. Soc. Jpn. **53**, 3765 (1984).